Adsorption (2011) 17: 573–581
DOI 10.1007/s10450-011-9330-x

Synthesis, characterization and in vitro cytotoxicity of Pt-TiO_2 nanoparticles

T. López · M. Alvarez · R.D. González · M.J. Uddin · J. Bustos · S. Arroyo · A. Sánchez

Received: 18 December 2010 / Accepted: 28 January 2011 / Published online: 12 February 2011

Abstract The adverse toxicological profile of cisplatin (cis-dichlorodiammineplatinum (II)), characterized by nephrotoxicity and neurotoxicity is the main factor that limit the clinical usefulness of this antineoplastic drug, specifically the possibility of applying it in effective high-dose regimens. In order to overcome these disadvantages, many efforts in the search for new drugs have been made. Due to this particularity, we obtained via sol–gel process $Pt(acac)_2$–TiO_2 (NPt) nanostructured materials with antitumoral activity to be used as an alternative in the treatment of cancer tumors. The biocatalysts were prepared by the sol–gel route using the complex $Pt(acac)_2$. Sol–gel parameters were controlled in order to obtain high platinum dispersion and particles in the nano-size range. TEM, FTIR, N_2 adsorption and XPS characterization studies of the samples were carried out. In order to investigate interactions between the biocatalyst and DNA, agarose gel electrophoresis was performed, and we observed the formation of DNA adducts. 45 minutes after contact, NPt completely degraded the DNA (cisplatin 120 minutes). These results demonstrate that using a metal supported and dispersed over an inorganic biocompatible oxide, can be effectively used in the treatment of localized tumors.

Keywords Sol–gel process · Nanomedicine · Glioblastoma multiforme · DNA electrophoresis

Abbreviations
GBM Glioblastoma multiforme
NPt platinum-titania nanoparticles

1 Introduction

Nanotechnology is an area of science devoted to the design, construction, and utilization of functional structures on the nanometer scale. There are numerous applications for nanotechnology referred as "nanomedicine" by the National Institute of Health (Bethesda, MD, USA): biosensing (Pirozzi et al. 2009; Kaushik et al. 2009), biological separation (Gültekin et al. 2009), molecular imaging (Song et al. 2009) and anticancer therapy (Zhou et al. 2009; Kuo et al. 2009), these applications are related with their novel properties and functions that differ from their bulk counterparts (Gao and Xua 2009). Although all these nanomedical devices allow new opportunities for many diseases, their practical application has been limited by problems with toxicity, instability, and/or lack of selectivity.

To overcome these limitations, researchers have made several modifications by physically or chemically anchoring biocompatible polymers on the surfaces of diagnostic and treatment nanomedicines (Patil et al. 2009). The surface

T. López · J. Bustos
Departamento de Atención a la Salud, Universidad Autónoma Metropolitana Xochimilco, Calz. Del Hueso 1100, Villa Quietud, Coyoacán, 04960, México, D.F., Mexico

T. López (✉) · M. Alvarez · S. Arroyo
Laboratorio de Nanotecnología, Instituto Nacional de Neurología y Neurocirugía, Av. Insurgentes sur 3877, La Fama, 14269, Tlalpan, México, D.F., Mexico
e-mail: tessy3@prodigy.net.mx

T. López · R.D. González · M.J. Uddin
Department of Chemical Engineering, Tulane University, New Orleans, LA 70118, USA

A. Sánchez
Laboratorio de Patología experimental, Instituto Nacional de Neurología y Neurocirugía, Av. Insurgentes sur 3877, La Fama, 14269, Tlalpan, México, D.F., Mexico

modification of nanoparticles with hydrophilic groups reduces the interfacial energy in an aqueous environment, thus preventing unwanted aggregation due to secondary interactions between nanoparticles (Qiu and Wang 2008; Park et al. 2010). In addition, the surface functionalization of these particles with hydrophilic groups may the recognition by proteins and cells in the body, allowing the nanomaterials to circulate in the blood for a longer period of time and increasing the possibility that it will reach the target site.

Cancer cells often display increased cell surface expression of proteins that may be found at low levels on normal cells (tumor-associated antigens), as well as proteins that are found exclusively on cancer cell surfaces (tumor-specific antigens). Active drug targeting is usually achieved by chemical attachment to a targeting component that strongly interacts with antigens (or receptors) displayed on the target tissue, leading to preferential accumulation of the drug in the targeted organ, tissue, or cells. The use of a targeting moiety not only decreases adverse side effects by allowing the drug to be delivered to the specific site of action, but also facilitates cellular uptake of the drug by receptor mediated endocytosis, which is an active process requiring a significantly lower concentration.

In the search of new therapeutic cancer drugs, platinum complexes are very interesting due to the anticancer demonstrated activity of platinum (Galanski et al. 2004; Jadhav et al. 2010; Pang et al. 2007). Recent studies have shown that nanoparticles of inorganic polymers such as SiO_2 and TiO_2 used as catalytic supports of platinum complexes can interact with cancer cells (López et al. 2008, 2010; Trewyn et al. 2008; Liu et al. 2010; Chen et al. 2007; Zhu et al. 2010). In the present work we obtained NPt nanoparticles, using a chelate agent as solvent, these nanoparticles were characterized by physicochemical techniques and tested for in vitro activity against DNA.

2 Experimental

2.1 NPt synthesis

$Pt(acac)_2-TiO_2$ (NPt) nanoparticles were obtained by modifying the previously reported synthesis (Sánchez et al. 1996), using Titanium (IV) butoxide (Sigma-Aldrich, 97%) as precursor, acetylacetone as solvent and without hydrolysis catalyst. Two samples were prepared: TiO_2 reference and NPt under same stirring, temperature and pH condition. In the case of NPt, the appropriate amount of $Pt(acac)_2$ (Sigma-Aldrich, 97%) was dissolved in acetylacetone in order to obtain 1% mol of Platinum. The samples were dried at 70 °C and crushed for further analysis (PCT/IB2009/006079-june29.06.2009).

2.2 Characterization

2.2.1 FTIR

The samples were characterized by FTIR spectroscopy using a FTIR IR Affinity-1 spectrophotometer (Shimadzu). The samples (5%wt) were pressed together with KBr, into wafers (100 mg) for their analysis.

2.2.2 UV-Vis spectroscopy

The spectra of the powders were collected in a Cary-1 Varian spectrophotometer with integrating sphere from 200 to 800 nm. The samples were analyzed as obtained without any treatment.

2.2.3 Electronic microscopy

Scanning electron microscopy (SEM) was performed on a Hitachi-4800 Field Emission Scanning Microscope operated at 3 kV to investigate porous morphology and nanostructure. The cryogenic conditions maintained with a constant liquid nitrogen flow through the SEM analysis chamber. The aqueous phase from the top surface of the bubble shape frozen sample removed by maintaining temperature gradient (10 °C) for 5 min between the sample and the anticontaminator plate. The sample was then transferred under the protection of high vacuum into the cryo-FESEM microscope chamber and imaged at an accelerating voltage of 2 kV and at a working distance of 5 to 6 mm.

The high magnification Transmission Electron Microscopy (TEM) images were obtained using TEM; JEOL 2010, operated at 120 kV voltage equipped with energy dispersive spectroscopic (EDS) microanalysis system (OXFORD). The images were obtained using a CCD Mega Vision (III) camera.

2.2.4 XRD

The X-ray diffraction (XRD) patterns were obtained using a Brucker D-5000 diffractometer equipped with Cu-Kα radiation of wavelength of 1.5418 Å. The accelerating voltage and the applied current were 45 kV and 40 mA, respectively.

2.2.5 XPS

The spectra were collected in a VSW Scientific Instrument HA100 with 285 lens, the excitation source was Al K_α ($E = 1486.6$ eV), the instrument is equipped with spherical sector analyzer; the analyzer pass energy was 22 eV and resolution of 0.6 eV. Calibration and reference spectra were taken the same day. A Shirley function was applied for background correction.

2.2.6 N_2 adsorption measurements

Adsorption measurements were made in a BELSORP II (Bel Japan Inc.) equipment using N_2 as adsorbate (77 K). Prior adsorption the porous samples were outgassed under high vacuum ($<1\times10^{-6}$ Torr) at 100°C. Specific surface areas were calculated using the BET equation[30] and pore size distributions were obtained by the BJH method, pore size distribution was estimated using BJH method.

2.2.7 In vitro DNA test

Total DNA was extracted from C6 cells using the Qiagen kit. The DNA concentration was measured using a Biorad biophotometer. 2 µL of a DNA solution (500 µg/mL) was mixed with 2 µL of the nanoparticle solution (100 mg/500 µL) and incubated at 37°C for different times. Following incubation, electrophoresis in 1% agarose gel was performed at 120 V for 1 hr. The gels were stained with ethidium bromide and images were acquired using a Biorad GelDoc.

2.2.8 In vivo antitumor activity

C6 glioma cells were cultured using DMEM containing 10% FBS, 10000 U penicillin/10 mg/ml estreptomycin at 37°C in 5% CO_2 atmosphere. The cells were washed with PBS sterile and added 800 ml of trypsine (0.05%, EDTA) for each box. The cells were stained in trypan blue (4%), and counted. 1×10^6 cells were suspended in a vial and injected in a hole drilled into the left side of the skull (Bregma AP = 1.6 mm, Lateral = 3.0, Vertical = 2.0 mm) of male Wistar rats (200–250 g) previously anesthetized (80 mg/kg ketamine and 10 mg/kg xylazine) by means of stereotaxic surgery. The animals were allocated in 3 groups ($n = 10$) namely Control (A), NPt-ref (B) and NPt (C). One week after cell injection, the animals were administrated with compressed cylinders made of NPt-ref (group B) and NPt (group C) materials in the same coordinates and with the same surgical procedure. In order to evaluate in vivo antitumor activity the animals were monitored in the following months and then sacrificed to remove the brain for further histological study (Hematoxiline-Eosine stain).

3 Results and discussion

3.1 FTIR and UV-vis spectroscopy

It has been reported that sol–gel method is a suitable method to obtain supported catalysts with highly metal dispersion (Hu et al. 2006; Lambert and Gonzalez 1998). Moreover, modification of TiO_2 surface can be achieved through addition of functionalizing agents as well as by using a variety of solvents (Schubert 2005). In our case, we report on the synthesis of functionalized TiO_2 materials with acetylacetone groups. FTIR spectra of the sol–gel samples NPt and NPt-ref as well as $Pt(acac)_2$ are showed on Fig. 1. In the high energy region, we can observe for NPt and NPt-ref samples, the presence of a wide band around 3400 cm^{-1}, characteristic of sol–gel materials. The appearance of two additional bands in the NPt sample, that are higher than the observed in NPt-ref and are not presented in platinum compound spectrum, involved three different vibrations associated with vibrations of O–H bonds due to the presence of water, the formation of hydrogen bonds between Ti–OH and acac groups. In the low energy region (Fig. 1b), NPt and NPt-ref spectra showed typical doublet around 1550 cm^{-1} associated with the Ti–O–(acacaH) vibrations, this is supported by the band observed at 441 cm^{-1} (Klein 1988; Guzmán et al. 2007). Between 1300 and 500 cm^{-1} all the spectra are similar and exhibits the corresponding bands to C–H vibrations; the band observed at 474 cm^{-1} in the platinum compound corresponding to Pt–O vibrations, appears like a small shoulder in the band centred at 439 cm^{-1} in the NPt and NPt-ref spectra. In these samples a band located at ca. 830 cm^{-1} appears, this band is due to the presence of C–H bond vibrations due to the interaction between titania surface and acetylacetonate groups (Sánchez et al. 1996). The obtained spectra showed that complexant ligands behave as terminal functional groups, and indicates that the materials were efficiently functionalized. We suggest that C=O or C–O– of the platinum acetylacetonate, linked to the titania net, through the hydroxyl groups of the surface and desorbing H_2O. Then, the loaded platinum is mainly over the surface but some platinum atoms can be incorporated into titania net replacing some titanium atoms, moreover the use of acetylacetone as solvent, leads to the formation of some

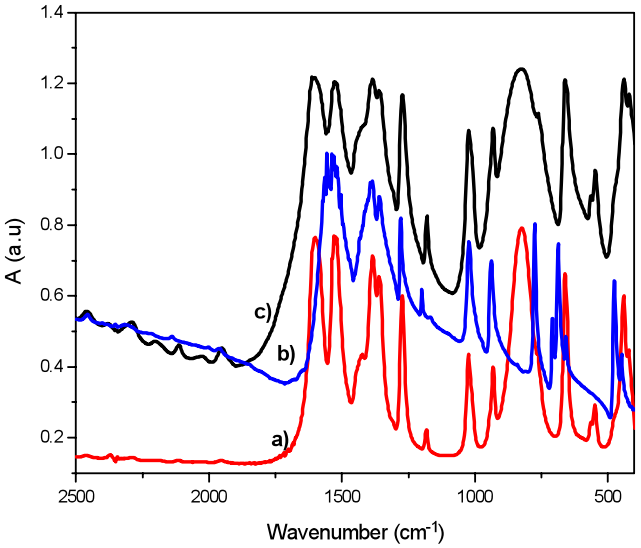

Fig. 1 FTIR of the KBr supported samples (*a*) NPt-ref, (*b*) Pt compound and (*c*) NPt

$TiO(acac)_2$ as can be observed by XRD, mainly in the surface of the materials.

To confirm the information obtained from FTIR characterization, UV-visible spectra of the samples were collected (Fig. 2). The absorption of the Ti4+ tetrahedral symmetry normally appears at around 350 nm (Choi and Kang 2007). In the case of NPt-ref, the fundamental absorption edge of TiO_2 appeared in the UV region at about 304 nm that corresponds to charge transfer from O 2p to Ti 3d orbitals. The maximum absorption for NPt and was observed at 304 nm too with an additional band at 335 nm. UV-vis spectrum of pure $Pt(acac)_2$ is also displayed in Fig. 2 for comparison. The presence of a shoulder around 400 nm in NPt sample showed the incorporation of platinum acetylacetonate into NPt material.

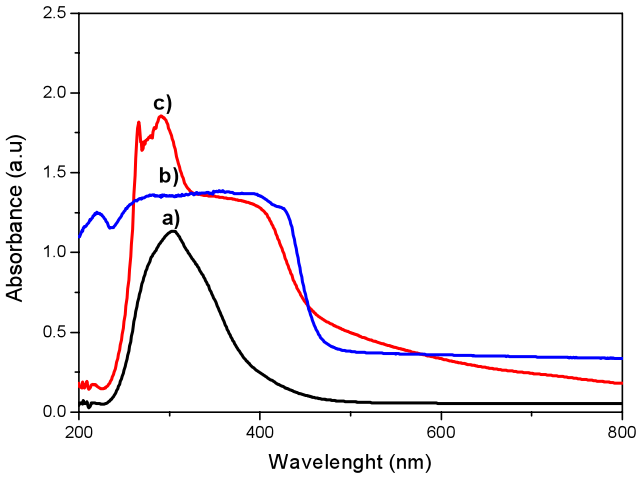

Fig. 2 UV-Vis spectra of (*a*) NPt-ref, (*b*) Pt compound and (*c*) NPt samples

3.2 Electronic microscopy

Morphology of the NPt nanoparticles is showed in Fig. 3. FESEM showed agglomerates formation for both samples. When NPt sample was analyzed by cryo-FESEM we observed that NPt can be dispersed in water very well (Fig. 3c and 3d). These agglomerates are formed by very tiny particles as TEM confirmed, with particles size of less than 10 nm.

According to the TEM (Fig. 4), particle size of NPt nanomaterial is very small (from 1 to 2 nm). On the other hand, following reduction, the observed particle size is much larger (from 50 nm upwards). The result is that on the original non-reduced sample the Pt is mono-dispersed (high Pt dispersion) but not so on the reduced material, that exhibits a low dispersion. The method of synthesis allows us to obtain this high dispersion due to the inclusion of platinum at the beginning of the process. It has been extensively reported that highly dispersed metal enhances its catalytic activity (Lambert et al. 2009; Bosch et al. 1993). Moreover, when particle size of supported platinum is very small, as well as the oxidation state increases considerably selectivity of the catalyst.

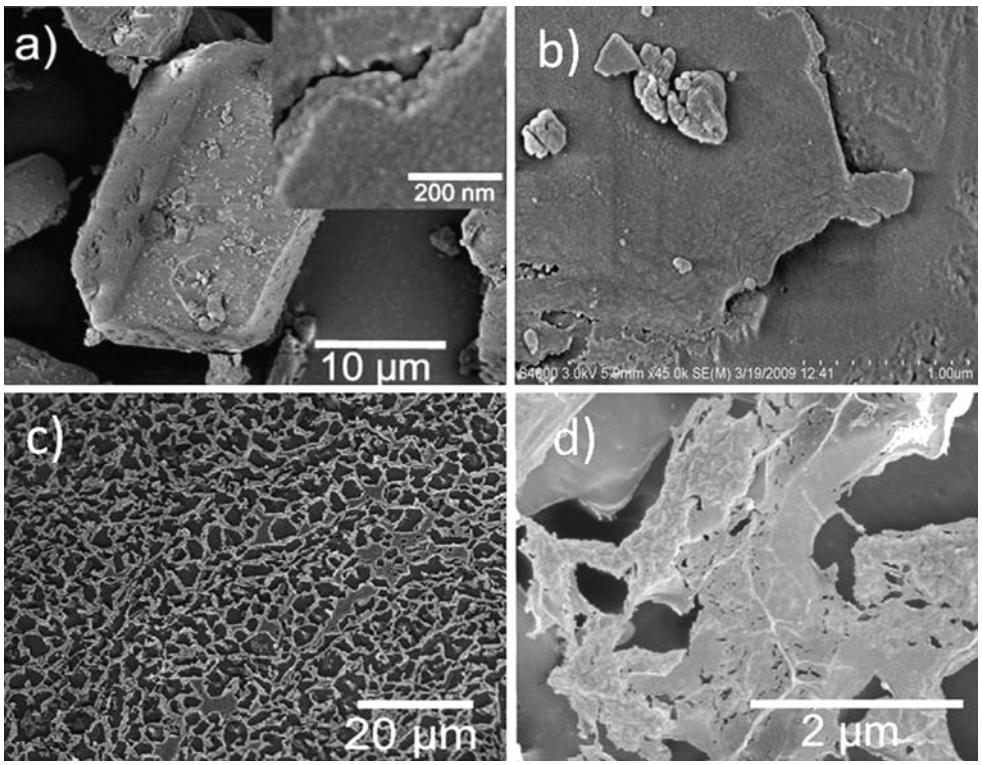

Fig. 3 FESEM images of (**a**) NPt (**b**) higher amplification, cryo-FESEM images of (**c**) NPt dissolved and vitrified in H_2O and (**d**) higher magnification

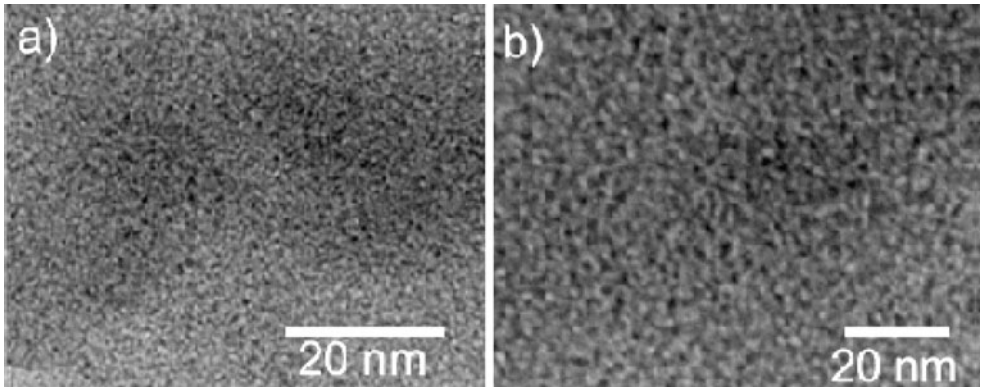

Fig. 4 TEM of NPt material

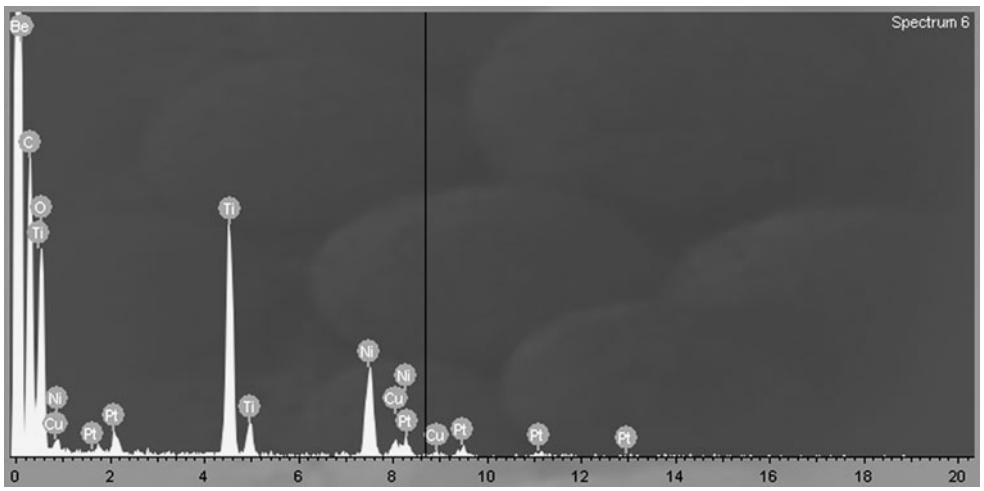

Fig. 5 EDX spectra of NPt obtained by SEM

EDX analysis showed the composition of NPt material (Fig. 5). As it can be observed, the material is mainly composed by Ti, O, C and Pt. The large amount detected of carbon is due to the presence of acetylacetonate ligands, that are forming mono or bidentate ligands with the oxygen atoms of octahedral titania.

3.3 XRD

In order to study the influence of $TiO(acac)_2$ compound, the NPt sample was reduced under H_2 at 500 °C during 4 hours. XRD measurements (Fig. 6) showed that in NPt sample the presence of $TiO(acac)_2$ can be detected (this information is in agreement with the observed by FTIR). When the sample was reduced, anatase and rutile signals are observed and $TiO(acac)_2$ signals disappear. Before reducing the sample, NPt material showed a crystallite size of 47 nm. Once the NPt is reduced anatase is the main crystalline phase (ca. 88%) but some rutile is present (ca. 12%) and crystallite size are 17 and 20 nm respectively.

Adsorption isotherms of NPt, NPt-red and NPt-ref were measured in order to obtain information about textural properties of the samples (Fig. 7). The form of isotherms is very close and is a type IV according to IUPAC classification, this is characteristic of mesoporous solids. NPt-ref and NPt-red samples exhibited isotherm with no hysteresis, these materials exhibits a very small surface area (2.5 and 15.6 $m^2\ g^{-1}$ respectively) since the pores are both meso and micropores, in this case the limiting uptake is governed by the accessible micropore volume rather than by the internal

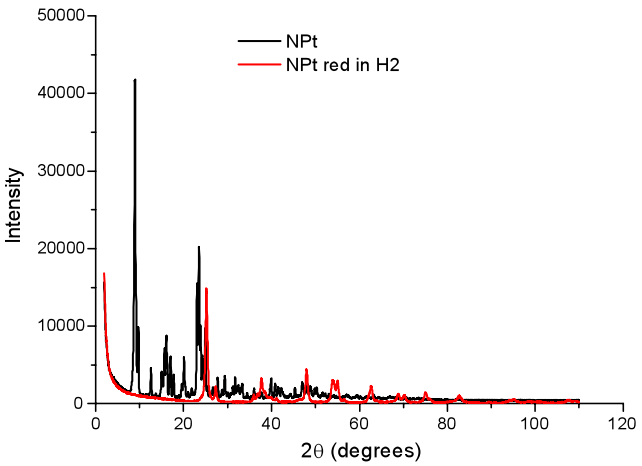

Fig. 6 XRD patterns of NPt and reduced NPt

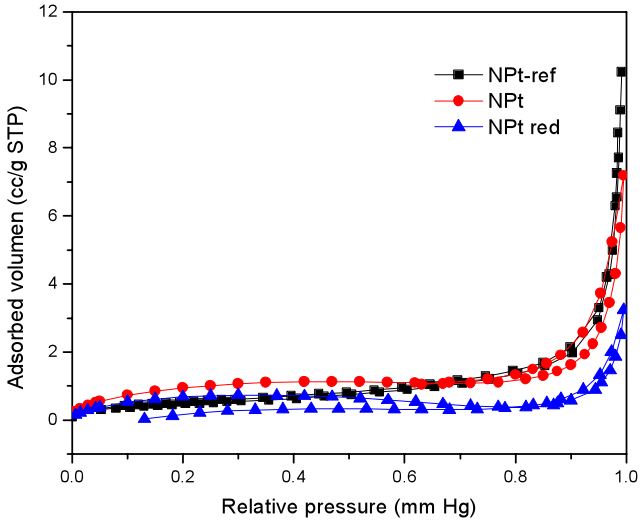

Fig. 7 Adsorption-desorption N_2 isotherms of NPt and NPt-reference. The *inset* corresponds to particle size distribution of both samples

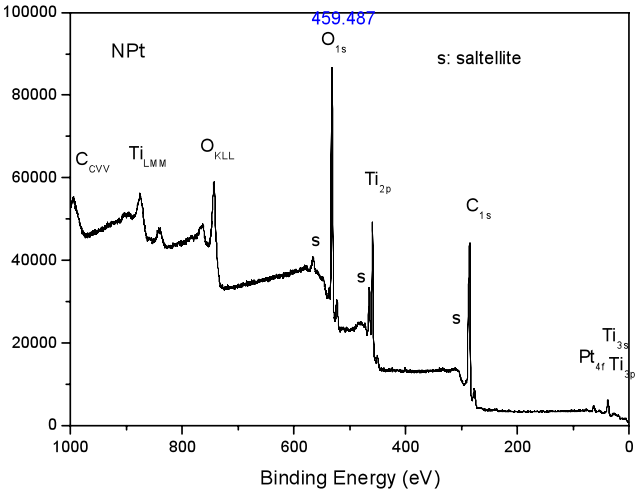

Fig. 8 Full XPS spectrum of NPt

surface area. For the NPt material something similar happens ($S_{BET} = 2.5\ m^2\ g^{-1}$) but isotherm in this case showed hysteresis type HI, associated the presence of agglomerates and this is in agreement with the observed by electronic microscopy. The low BET values are related with the presence of agglomerates of particles too. This could be explained by the presence of a large amount of acetylacetone groups linked to the surface through Ti–OH groups and Ti–O of the particles that limits the access to N_2 atoms. Here, incorporation of acetylacetone during the synthesis of the materials promotes the formation of these agglomerates as SEM images showed.

As mentioned before, one of the most important features for catalytic activity is related with the chemical species present over the support. The full XPS spectrum for NPt nanomaterial is showed in Fig. 8. We observed the presence of Ti, O, Pt and C elements.

3.4 XPS

XPS spectra of both NPt and NPt-reduced samples are showed in Fig. 9. The Ti 2p spectrum, displays the spin–orbit split lines to Ti $2p_{3/2}$ (459.67 eV) and Ti $2p_{1/2}$ (465.46 eV), $\Delta 2p_{1/2}$–$2p_{3/2}$ for the NPt nanomaterial is 5.79 eV indicating the presence of Ti(IV) species. The C 1s xps spectrum is in Fig. 9 and shows two peaks at 285.63 and 287.7 eV, which correspond to amorphous carbon not bonded to TiO_2 and to C=O from the organic solvent respectively. The peak positions of Ti $2p_{3/2}$ and O 1s in the XPS spectrum can be assigned to the Ti–O bonds of TiO_2.

Regarding to the O 1s signal, we observed that for NPt material, this signal is centered at 532.2 eV, and is slightly shifted from the reported for conventional TiO_2 commonly around 529 eV; this signal is formed by two bands: one located at 531.02 and the other one at 532.51 eV, indicating different oxygen species The first corresponds to oxygen bonded in TiO_2 and the last one to oxygen in the carbonyl group of acetylacetone ligand (Beamson and Briggs 1992). The environment of these oxygen species are mainly Ti atoms from TiO_2, hydrogen from hydroxylated surface and to carbon atoms. When the sample is reduced, the O 1 s signal showed that oxygen species from C=O are absent of the material, and this is due to the thermal treatment when the sample is reduced.

In the platinum XPS spectra we show the $4f_{7/2}$ and $4f_{5/2}$ signals at 74.13 and 77.26 correspondingly. These signals appears at 71.4 and 74.95 in the reduced sample where the oxidation state is Pt(0). This is indicative of higher oxidation state in the NPt nanomaterial, probably a combination of Pt(II) and Pt(IV) species.

3.5 In vitro DNA degradation

The obtained nanoparticles were tested in vitro directly with DNA of cancer cells (C6 cell line). A suspension of nanoparticles was incubated directly with DNA and in a first experiment we observed a total DNA degradation after 6 hours. In a more detailed study (Fig. 10) we follow DNA degradation at shorter periods of time. We observed that at $t = 30$, NPt (lane 5) begins to interact with DNA since the band becomes to disappear even before than cisplatin (a well known antitumor agent). At $t = 60$, all the DNA was degraded while the equivalent amount of cisplatin reached this after 180 minutes of incubation. This could be explained essentially by the functionalized surface of the NPt material. Here we observed that even bare reference (without platinum) degraded DNA after 24 hours. The presence of $TiO(acac)_2$ formed during the synthesis of NPt, gives additional actives sites to charge deficient sites in the surface of TiO_2 for interaction with DNA bases.

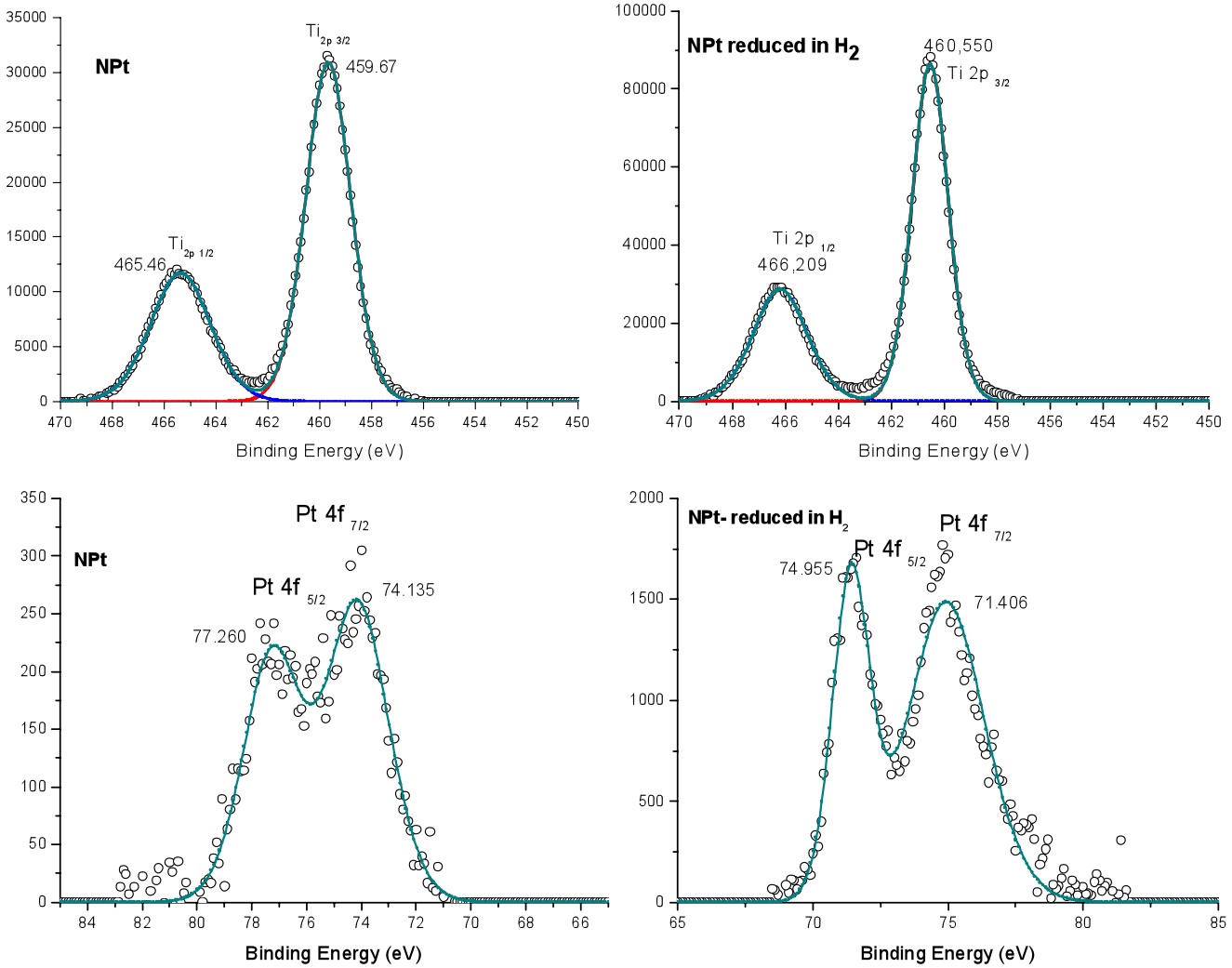

Fig. 9 XPS spectra of Ti 2p and Pt 4f from NPt and NPt-reduced in H_2 samples

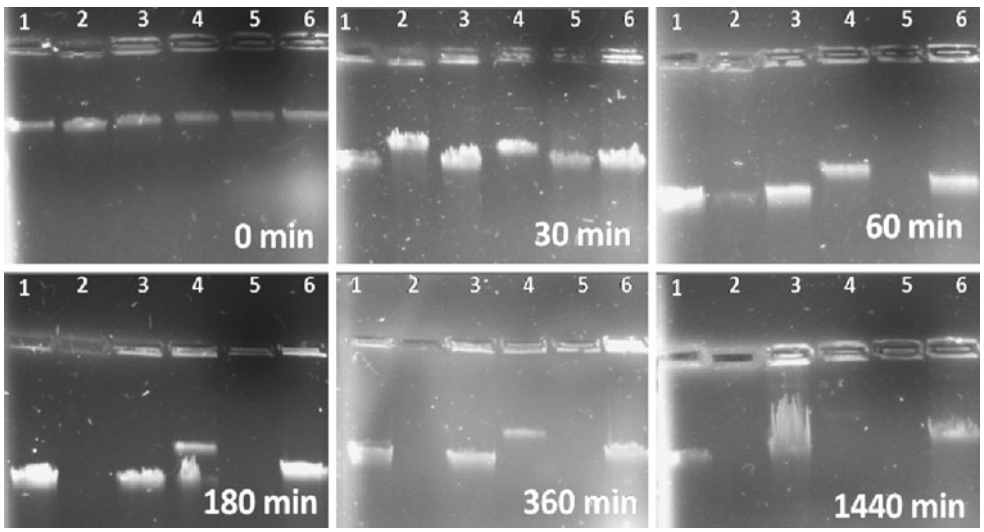

Fig. 10 Electrophoretograms at different times. Lanes *1*. Control (+), *2*. cisplatin; *3*. NPt-Ref, *4*. cisplatin-TiO_2, *5*. NPt, *6*. NPt-red

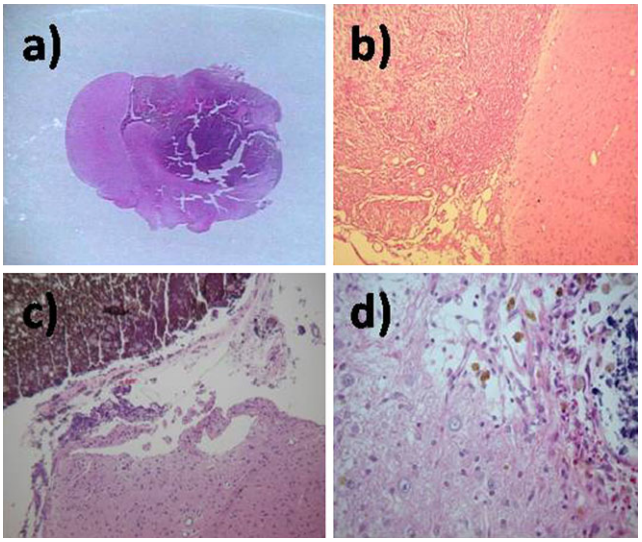

Fig. 11 H-E staining of processed brain tissue (**a**) natural evolution of induced GBM after 26 days, (**b**) interface tumor-normal tissue, (**c**) post treatment (4 months), (**d**) higher amplification

3.6 In vivo antitumor activity

In order to confirm in vitro DNA activity, an animal model using Wistar rats was performed. Because of high aggressiveness glioblastoma multiforme (GBM) is one of the tumors with poorest prognosis and there is no effective treatment to date. For this reason we use a GBM model induced in rats, inoculating C6 cell line. Although rodent GBM characteristics are not the same than human GBM, has been a good approximation for testing purposes. In our experiment, once the animals developed the intracranial tumor, and no treatment was administrated the survival was no longer than 30 days (control group). Due to the size of the animals, the tumor was induced in motor cortex in order to evaluate and determine with observation any change in motor skills of the animals. An interesting result was observed when NPt was administrated. A cylinder made of NPt (5 mg) was surgically placed into the tumor by stereotaxic surgery. Fourth months later, the animals were sacrificed and the brains processed for pathologic analysis. Hematoxiline-Eosine (H-E) stain photographs of the processed brains are shown in Fig. 11. In the animals of the control group, we can observe the free evolution of the tumor with some of the main characteristics of GBM like high cell proliferation and vascularization as well as necrosis (a, b). In the other hand, the tumors treated with NPt showed lower growth and less invasiveness. In Fig. 11c treated tumor image shows the presence of the compressed NPt device, we can observe that surrounding tissue is formed by normal cells (no tumor cells appears), meningothelial hyperplasia was observed between the material and the normal cells. We assume that the tumor growth was slow down due to interaction between the NPt and cancer cells, avoiding its spread. At the same time, we must notice that since the NPt cylinder remains fixed, antitumor action is strongly related with surface contact and more experiments need to be carried in order to improve the via of administration that allow an optimal interaction between cancer cells and NPt material.

4 Conclusions

We synthesized NPt nanoparticles, with high dispersed platinum and functionalized surface. Addition of a chelate agent as acetylacetone brings new features to the supported nanoparticles. Formation of titanium acetylacetonate due to synthesis conditions leads to the anchoring of this chemical compound to the surface of TiO_2. Although low surface area values were observed for the obtained nanomaterials this parameter not influences in DNA degradation, since NPt showed high interaction in a shorter time than a conventional chemotherapeutic drug (cisplatin). However, it seem that the oxidation sate of platinum is a more relevant parameter, since Pt(0) of the NPt-reduced sample showed lower activity than NPt where platinum exhibits a higher oxidation state. These results suggest that NPt nanoparticles could be used as antitumor agent with the main advantage that cytotoxic agent (platinum) remains anchored to the support, as well as the acetylacetonate groups, decreasing its concentration into the body and diminishing the adverse side effects.

Acknowledgements To CONACyT-FONCYCT project 96095, CONACyT México, ICyTDF, Tulane University, Universidad Autónoma Metropolitana and National Institute of Neurology and Neurosurgery-México. Authors are grateful to Dr. D. Rembao for technical assistance.

References

Beamson, G., Briggs, D.: High Resolution XPS of Organic Polymers. The Scienta ESCA 300 Database. Wiley, Chichester (1992)

Bosch, P., Lopez, T., Lara, V.-H., Gomez, R.: Pt/SiO_2 catalysts: a comparison of the impregnation and the sol–gel methods. J. Mol. Catal. **80**, 299–306 (1993)

Chen, G., Zhao, J., Liu, X., Gao, G., Huang, J., Li, G.: Electrochemical sensing DNA damage with nano-titanium dioxide and repair with a medicinal herb species resveratrol. J. Biotechnol. **127**, 653–656 (2007)

Choi, H.-J., Kang, M.: Hydrogen production from methanol/water decomposition in a liquid photosystem using the anatase structure of Cu loaded TiO_2. Int. J. Hydrog. Energy **32**, 3841–3848 (2007)

Galanski, M., Baumgartner, C., Meelich, K., Arion, V.B., Fremuth, M., Jakupec, M.A., Schluga, P., Hartinger, C.G., Keyserlingk, N.G., Keppler, V.K.: Synthesis, crystal structure and pH dependent cytotoxicity of *(SP-4-2)*-bis(2-aminoethanolato-κ^2N,O)platinum(II)—a representative of novel pH sensitive anticancer platinum complexes. Inorg. Chim. Acta **357**, 3237–3244 (2004)

Gao, J., Xua, B.: Applications of nanomaterials iside the cells. Nano Today **4**, 37–51 (2009)

Gültekin, A., Diltemiz, S.E., Ersöz, A., Sarıözlü, N.Y., Denizli, A., Say, R.: Gold–silver nanoclusters having dipicolinic acid imprinted nanoshell for *Bacillus cereus* spores recognition. Talanta **78**, 1332–1338 (2009)

Guzmán, A.M., Fernández, A.M., Franco, Y., Bautista, J.H., Rodríguez Páez, J.E.: Rev. Acad. Colomb. Cienc. **31**(121), 529–536 (2007)

Hu, L., Boateng, K.A., Hill, J.M.: Sol–gel synthesis of Pt/Al_2O_3 catalysts: effect of Pt precursor and calcinations procedure on Pt dispersion. J. Mol. Catal. A, Chem. **259**, 51–60 (2006)

Jadhav, V.B., Jun, Y.J., Song, J.H., Park, M.-K., Oh, J.H., Chae, S.W., Kim, I.-S., Choi, S.J., Lee, H.J., Sohn, Y.S.: A novel micelle-encasulated platinum(II) anticancer agent. J. Control. Release **147**, 144–150 (2010)

Kaushik, A., Solanki, P.R., Ansari, A.A., Sumana, G., Ahmad, S., Malhotra, B.D.: Iron oxide-chitosan nanobiocomposite for urea sensor. Sens. Actuators B, Chem. **138**, 572–580 (2009)

Klein, L.C. (ed.): Sol–gel technology for thin films, fiber performs, electronic and especiality shapes. Noyes, Park Ridge (1988)

Kuo, T.R., Wu, C.-L., Hsu, C.-H., Lo, W., Chiang, S.-J., Lin, S.-J., Dong, C.-Y., Chen, C.-C.: Chemical enhancer induced changes in the mechanisms of transdermal delivery of zinc oxide nanoparticles. Biomaterials **30**, 3002–3008 (2009)

Lambert, C.K., Gonzalez, R.D.: The importance of measuring the metal content of supported metal catalysts prepared by the sol–gel method. Appl. Catal. A, Gen. **172**, 233–239 (1998)

Lambert, S., Job, N., D'Souza, L., Ribeiro, Pereira M.F., Pirard, R., Heinrichs, B., Figuiredo, J.L., Pirard, J.-P., Regalbuto, J.R.: Synthesis of very highly dispersed platinum catalysts supported on carbon xerogelsby the strong electrostatic adsorption method. J. Catal. **261**, 23–33 (2009)

Liu, L., Miao, P., Xu, Y., Tian, Z., Zou, Z., Li, G.: Study of Pt/TiO_2 nanocomposite for cancer-cell treatment. J. Photochem. Photobiol., B Biol. **98**, 207–210 (2010)

López, T., Recillas, S., Guevara, P., Sotelo, J., Alvarez, M., . Odriozola, J.A.: Pt/TiO_2 brain biocompatible nanoparticles: GBM treatment using the C6 model in Wistar rats. Acta Biomater. **4**, 2037–2044 (2008)

López, T., Figueras, F., Manjarrez, J., Bustos, J., Alvarez, M., Silvestre-Albero, J., Rodríguez-Reinoso, F., Martínez-Ferre, A., Martínez, E.: Catalytic nanomedicine: a new field in antitumor treatment using supported platinum nanoparticles. In vitro DNA degradation and in vivo tests with C6 animal model on Wistar rats. Eur. J. Med. Chem. **45**, 1982–1990 (2010)

Pang, S.-K., Yu, C.-W., Au-Yeung, S., Ho, Y.-P.: DNA damage induced by novel demethylcantharidin-integrated platinum anticancer complexes. Biochem. Biophys. Res. Commun. **363**, 235–240 (2007)

Park, J.H., Lee, S., Kim, J.-H., Park, K., Kim, K., Kwon, I.C.: Polymeric nanomedicine for cancer therapy. Prog. Polym. Sci. **33**, 113–137 (2008)

Park, J.T., Seo, J.A., Ahn, S.H, Kim, J.H., Kang, S.W.: Surface modification of silica nanoparticles with hydrophilic polymers. J. Ind. Eng. Chem. **16**, 517–522 (2010)

Patil, Y.B., Toti, U.S., Khdair, A., Ma, L., Panyam, J.: Single step surface functionalization of polymeric nanoparticles for targeted drug delivery. Biomaterials **30**, 859–866 (2009)

Pirozzi, D., Fanelli, E., Aronne, A., Pernice, P., Mingione, A.: Lipase entrapment in a zirconia matrix: Sol–gel synthesis and catalytic properties. J. Mol. Catal., B Enzym. **59**, 116–120 (2009)

Qiu, J., Wang, G.-J.: Comparative study on modification of multiwalled carbon nanotubes by a hydrophilic polymer with different approaches. Appl. Surf. Sci. **254**, 5691–5694 (2008)

Sánchez, E., López, T., Gómez, R., Bokhimi, X., Morales, A., Novaro, O.: Synthesis and characterization of sol–gel Pt/TiO_2 catalysts. J. Solid State Chem. **122**, 309–314 (1996)

Schubert, U.: Chemical modification of titanium alkoxides for sol–gel processing. J. Mater. Chem. **15**, 3701–3715 (2005)

Song, C., Ye, Z., Wang, G., Jin, D., Yuan, J., Guan, Y., Piper, J.: Preparation and time-gated luminescence bioimaging application of ruthenium complex covalently bound silica nanoparticles. Talanta **79**, 103–108 (2009)

Trewyn, B.G., Nieweg, J.A., Zhao, Y., Lin, V.S.-Y.: Biocompatible mesoporous silica nanoparticles with different morphologies for animal cell membrane penetration. Chem. Eng. J. **137**, 23–29 (2008)

Zhou, L., Zhou, J.-H., Dong, C., Ma, F., Wei, S.-H., Shen, J.: Water-soluble hypocrellin A nanoparticles as a photodynamic therapy delivery system. Dyes Pigm. **82**, 90–94 (2009)

Zhu, X., Chen, Z., Zhang, X., Zhu, Z., Li, G.: Biomolecule-directed assembly of binary gold and titanium dioxide nanoparticles. J. Nanosci. Nanotechnol. **10**, 1021–1024 (2010)